energies

MDPI

Article

Determination of the Differential Capacity of Lithium-Ion Batteries by the Deconvolution of Electrochemical Impedance Spectra

Dongxu Guo [1], Geng Yang [1,*], Guangjin Zhao [2], Mengchao Yi [3], Xuning Feng [4,*], Xuebing Han [4], Languang Lu [4] and Minggao Ouyang [4]

1 Department of Automation, Tsinghua University, Beijing 100084, China; gdx16@mails.tsinghua.edu.cn
2 State Grid Henan Electric Power Research Institute, Zhengzhou 450052, China
3 College of Engineering, China Agricultural University, Beijing 100083, China
4 State Key Laboratory of Automotive Safety and Energy, Tsinghua University, Beijing 100084, China; hanxuebing@tsinghua.edu.cn
* Correspondence: yanggeng@tsinghua.edu.cn (G.Y.); fxn17@mail.tsinghua.edu.cn (X.F.); Tel.: +86-010-6279-2512 (G.Y.)

Received: 18 January 2020; Accepted: 14 February 2020; Published: 18 February 2020

Abstract: Electrochemical impedance spectroscopy (EIS) is a powerful tool for investigating electrochemical systems, such as lithium-ion batteries or fuel cells, given its high frequency resolution. The distribution of relaxation times (DRT) method offers a model-free approach for a deeper understanding of EIS data. However, in lithium-ion batteries, the differential capacity caused by diffusion processes is non-negligible and cannot be decomposed by the DRT method, which limits the applicability of the DRT method to lithium-ion batteries. In this study, a joint estimation method with Tikhonov regularization is proposed to estimate the differential capacity and the DRT simultaneously. Moreover, the equivalence of the differential capacity and the incremental capacity is proven. Different types of commercial lithium-ion batteries are tested to validate the joint estimation method and to verify the equivalence. The differential capacity is shown to be a promising approach to the evaluation of the state-of-health (SOH) of lithium-ion batteries based on its equivalence with the incremental capacity.

Keywords: lithium-ion battery; electrochemical impedance spectroscopy; distribution of relaxation times; differential capacity; joint estimation; state-of-health evaluation

1. Introduction

Electrochemical impedance spectroscopy (EIS) has been proven to be a powerful tool for the diagnosis of complex electrochemical systems, including lithium-ion batteries [1–6], fuel cells [7,8], and supercapacitors [9,10]. Electrochemical impedance spectroscopy has been widely used to characterize the polarization processes of lithium-ion batteries [11–14] and to investigate various prognostics and health management (PHM) methods [15–19]. Electrochemical impedance spectrum is generally analyzed by a carefully chosen equivalent-circuit model (ECM), which requires knowledge about the electrochemical processes that take place at the individual electrodes within the cell [20–23]. Comparison between EIS-based ECM and incremental capacity has been presented to identify and quantify the effects of degradation modes [24]. However, some non-ideal processes and the overlapping effects lead to a certain level of ambiguity of the ECM during the model identification [25–27]. This problem needs to be settled by the deconvolution of the EIS data with respect to the distribution of relaxation times (DRT) [28–32].

Considering the DRT offers an approach that does not rely on any prior knowledge of the investigated electrochemical system [33,34]. Therefore, the use of the DRT is regarded as a model-free approach for system identifications. The DRT method attempts to decompose the impedance of a capacitive electrochemical system into a continuous distribution of resistor-capacitor (RC) elements in the domain of relaxation times [35]. Good practices were reported in the context of the analysis of the impedance of solid oxide fuel cells (SOFCs) and high-frequency impedance of lithium-ion batteries [7,31,32,36]. For low frequencies, however, the differential capacity caused by diffusion processes is non-negligible, and thus, cannot be decomposed by DRT. Consequently, low frequencies limit the application of the DRT method to lithium-ion batteries [5,37–39].

For lithium-ion batteries, the differential capacitive tail, as shown in Figure 1, has to be considered at low frequencies. Consequently, the DRT method needs to be modified as it cannot characterize a pure capacitive behavior. Some amending methods have been proposed to estimate the differential capacity, such as the preprocessing method [12,28], the distribution function of differential capacity (DDC) method [39], the distribution of diffusion times (DDT) method [40], and the differential impedance analysis (DIA) method [41,42]. However, the differential capacity and the DRT are estimated separately, resulting in accumulative errors, thereby limiting the applicability of the DRT method to lithium-ion batteries.

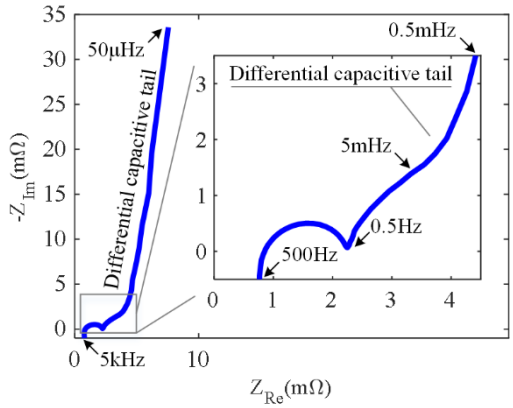

Figure 1. Electrochemical impedance spectrum of a lithium-ion battery with a differential capacitive tail, measured from 5 kHz to 50 μHz.

In this paper:

(1) A joint estimation method with Tikhonov regularization is proposed to simultaneously estimate the differential capacity and the DRT with the aim of minimizing the estimation errors and to obtain more information about the diffusion processes by EIS.
(2) Moreover, the equivalence of the differential capacity C_{DC} and the incremental capacity C_{IC} is proven in Section 2.
(3) Four types of commercial lithium-ion batteries are tested in Section 3 to validate the joint estimation method and to verify the equivalence of the C_{DC} and C_{IC}.
(4) Subsequently, the estimation results of the DRT and the C_{DC} are discussed in Section 4.
(5) In addition, an efficient state-of-health (SOH) evaluation method is demonstrated based on the relationship between the C_{DC} and the cell capacity in Section 4.
(6) The conclusions of the work are summarized in Section 5.

2. Theoretical

2.1. The Relationship between EIS and ICA

This section derives the relationship between the differential capacity C_{DC} identified by EIS and the incremental capacity C_{IC} obtained by ICA.

A typical EIS involves sweeping the excitation frequency with a sinusoidal voltage or current. In the EIS data, the complex impedance can be described by a frequency-dependent function:

$$Z(\omega) = \frac{U(\omega)}{I(\omega)} = R_{ohm} + R_{pol}(\omega) + \frac{1}{j\omega C_{DC}} \tag{1}$$

where ω is the angular frequency, $U(\omega)$ is the excitation voltage, $I(\omega)$ is the current response, j is the imaginary unit, R_{ohm} is the ohmic resistance, and $R_{pol}(\omega)$ is the polarization resistance. The differential capacity C_{DC} can be extracted theoretically by processing the limit at extremely low frequencies:

$$C_{DC} = \lim_{\omega \to 0} \frac{1}{j\omega\left(\frac{U(\omega)}{I(\omega)} - R_{ohm} - R_{pol}(\omega)\right)} \approx \lim_{\omega \to 0} \frac{Q(\omega)}{U(\omega)} = \frac{dQ}{dU} = C_{IC} \tag{2}$$

where $\frac{dQ}{dU}$ is the incremental capacity [43,44], denoted as C_{IC}. The equivalence of the C_{DC} and C_{IC} can be proved by Equation (2). The detailed derivation is given in Appendix A. Figure 2 gives a graphical interpretation of the relationship between C_{DC} and C_{IC} for a better understanding of the equivalence. This equivalence relationship expands the applicability of EIS to lithium-ion batteries, given that C_{DC} and C_{IC} are equal. This is highly beneficial, since estimating C_{DC} by EIS in certain cases is more straightforward and time-efficient compared with the use of ICA to measure C_{IC}.

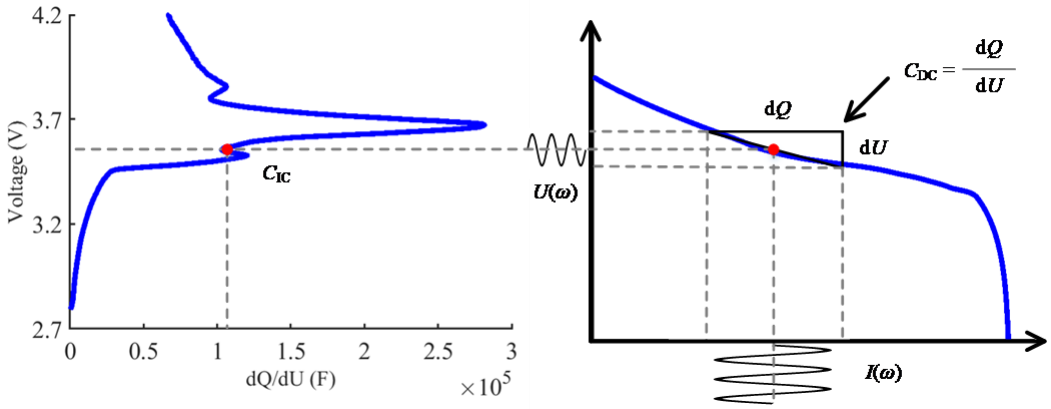

Figure 2. Relationship between C_{DC} and C_{IC}.

2.2. The Joint Estimation Method with Tikhonov Regularization

The value of the C_{DC} cannot be directly calculated by Equation (2) because the sweeping frequencies are discrete and have a lower limit. Therefore, the DRT method must be modified. The experimental data Z_{exp} measured at several sweeping frequencies were fitted by a model Z_{DRT} as follows [12,28,29,32]:

$$Z_{DRT}(\omega) = R_{ohm} + \int_0^{\infty} \frac{g(\tau)}{1 + j\omega\tau} d\tau \tag{3}$$

where τ represents the characteristic time constants and $g(\tau)$ represents the distribution of the polarization resistance. Furthermore, the differential capacity is non-negligible for lithium-ion batteries

as it contains information about the diffusion processes. Consequently, considering the differential capacity of lithium-ion batteries, the model Z_{DRT} was modified to obtain the following expression:

$$Z^{\mathrm{C}}_{\mathrm{DRT}}(\omega) = R_{\mathrm{ohm}} + \int_0^{\infty} \frac{g(\tau)}{1 + j\omega\tau} \mathrm{d}\tau + \frac{1}{j\omega C_{\mathrm{DC}}} \tag{4}$$

where $Z^{\mathrm{C}}_{\mathrm{DRT}}$ represents the DRT model considering the differential capacity C_{DC}. Subsequently, the discretized DRT model derived for Equation (3) in Ref. [29] can be reformulated into:

$$Z^{\mathrm{C}}_{\mathrm{DRT}}(\boldsymbol{\omega}) = R_{\mathrm{ohm}} + \left(\boldsymbol{A}^{'}\boldsymbol{x}\right)_{\mathrm{n}} + \left(\boldsymbol{A}^{''}\boldsymbol{x}\right)_{\mathrm{n}} + \frac{1}{j\boldsymbol{\omega} C_{\mathrm{DC}}} \tag{5}$$

where $\boldsymbol{\omega}$ is a column vector with n entries equal to the sweeping frequencies, $\boldsymbol{A}^{'}$ represents the approximation matrix of the DRT of the real part of the EIS data, $\boldsymbol{A}^{''}$ represents the approximation matrix of the DRT of the imaginary part of the EIS, and $\boldsymbol{x}$ represents the parameter vector for the DRT approximation. Then, the joint estimation function can be obtained by fitting the data with the improved discretized DRT model $Z^{\mathrm{C}}_{\mathrm{DRT}}(\boldsymbol{\omega})$, which implies the minimization of the following sum of squares:

$$J(\boldsymbol{x}) = \|\boldsymbol{\Omega}^{'}\left(R_{\mathrm{ohm}} \cdot \mathbf{1} + \boldsymbol{A}^{'}\boldsymbol{x} - \boldsymbol{Z}^{\mathrm{Re}}_{\mathrm{exp}}\right)\|^2 + \|\boldsymbol{\Omega}^{''}\left(\frac{1}{\boldsymbol{\omega} C_{\mathrm{DC}}} + \boldsymbol{A}^{''}\boldsymbol{x} - \boldsymbol{Z}^{\mathrm{Im}}_{\mathrm{exp}}\right)\|^2 \tag{6}$$

where $\boldsymbol{\Omega}'$ and $\boldsymbol{\Omega}''$ represent the frequency matrices of the DRT, $\mathbf{1}$ is a column vector with n entries all equal to 1, $\boldsymbol{Z}^{\mathrm{Re}}_{\mathrm{exp}}$ is the real part of the experimental data, and $\boldsymbol{Z}^{\mathrm{Im}}_{\mathrm{exp}}$ is the imaginary part of the experimental data. Implementation of the traditional DRT method is well established in the literature [7,12,28,29,38]. Hence, in the present work, we extend the traditional DRT to cover the C_{DC} part of the curve and perform a joint estimation. So, we only provide the modified optimization function to account for the C_{DC} based on Equation (6) as follows:

$$\min\left\{J(\boldsymbol{x}) = \|\boldsymbol{\Omega}'\left(R_{\mathrm{ohm}} \cdot 1 + \boldsymbol{A}'\boldsymbol{x} - \boldsymbol{Z}^{\mathrm{Re}}_{\mathrm{exp}}\right)\|^2 + \|\boldsymbol{\Omega}''\left(\frac{1}{\boldsymbol{\omega} C_{\mathrm{DC}}} + \boldsymbol{A}''\boldsymbol{x} - \boldsymbol{Z}^{\mathrm{Im}}_{\mathrm{exp}}\right)\|^2 + \lambda \boldsymbol{x}^{\mathrm{T}}\boldsymbol{M}\boldsymbol{x}\right\} \tag{7}$$

where λ is the regularization coefficient and $\boldsymbol{M}$ is the regularization matrix, which is derived in Ref. [29]. The problem stated in Equation (7) is the well-known Tikhonov regularization problem whose solution can be obtained by various numeric algorithms [29,38,45,46]. Then, the ohmic resistance R_{ohm}, the differential capacity C_{DC}, and the parameter $\boldsymbol{x}$ of the DRT can be simultaneously estimated by minimizing $J(\boldsymbol{x})$ in Equation (7).

3. Experimental

3.1. The Test Conditions

Table 1 lists the specifications of the four types of commercial lithium-ion batteries that were tested. The batteries will be henceforth referred to by the capitals A, B, C, and D for convenience. Two batteries had $LiNi_xCo_yMn_zO_2$ (NCM) cathodes, one had a $LiFePO_4$ (LFP) cathode, and one had a mixed cathode consisting of NCM and $LiMn_2O_4$ (LMO). Each battery had graphite anodes, marked as G in Table 1.

Table 1. Specifications of the tested lithium-ion batteries.

Battery	Cathode	Anode	Capacity (Ah)	Voltage Range (V)
A	NCM	G	3.2	2.5–4.2
B	NCM	G	4.8	2.5–4.2
C	LFP	G	20	2.0–3.65
D	NCM + LMO	G	24	2.5–4.2

The battery test platform is shown in Figure 3. The test platform consisted of a CT-4008-5V100A-NTFA tester (Neware, Shenzhen, China) a BTH-150C thermal chamber (DGBELL, Dongguan, China) an Autolab PGSTAT302N electrochemical workstation (Metrohm AG, Herisau, Switzerland) and a host computer. The Neware tester was used to charge and discharge the tested cells. The sampling frequency of the Neware tester was 1 Hz and its measurement accuracy was ±0.05% of its full scale. The thermal chamber provided the required ambient temperature with an accuracy of ±0.5 °C. The electrochemical workstation was used for EIS tests with a sampling frequency of 10 MHz. The host computer was used to control the tests and for data storage.

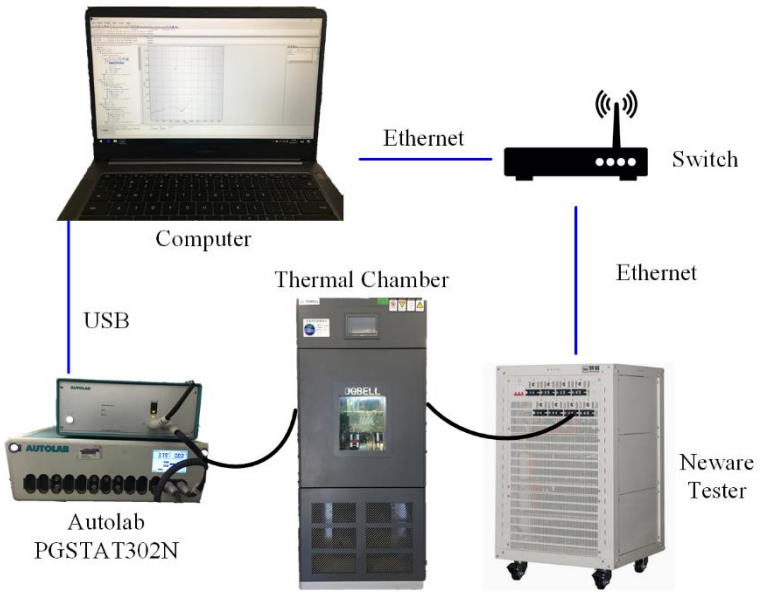

Figure 3. Configuration of the battery test platform.

3.2. *The Test Profiles*

Two test profiles were designed to verify the equivalence of the C_{DC} and C_{IC}. The profile for the EIS is described in Table 2 and the profile for the ICA is described in Table 3. EIS tests were conducted at 10% SOC intervals ranging from 100% to 0% SOC. The amplitude of the applied voltage in the EIS tests was 5 mV, and the frequency range is 2 kHz–2 mHz (60 points). For the ICA, the charging data of 1/20 C was adopted and processed by the probability density function (PDF) method [44].

Table 2. Test profile 1 for the EIS measurements.

Step No.	Step Name	Duration	Current	Cycle No.
1	Rest	180 min		
2	EIS test			
3	Discharge	18 min	1/3 C	
4	Cycle, step 1–3			10
5	Rest	180 min		
6	EIS test			
7	End			

Table 3. Test profile 2 for the ICA measurements.

Step No.	Step Name	Duration	Current	Condition
1	Rest	180 min		
2	Discharge		I = 1/20 C	V = upper limit
3	Rest	180 min		
4	Charge		I = 1/20 C	V = lower limit
5	End			

3.3. Aging Characterization of the Cells

Several D-type cells (denoted as D1–D7) were subject to cycling at 45 °C with a charge/discharge rate of 1 °C. D1 was a fresh cell, while D2 to D7 have been exposed to varying cycling, and hence, possessed varying *SOH*. In this paper, *SOH* is defined by assessing the actual capacity divided by the nominal capacity as follows [47–51]:

$$SOH = \frac{Q_{\text{act}}}{Q_{\text{nom}}} \tag{8}$$

where Q_{act} is the actual capacity in the cell's present condition and Q_{nom} represents the nominal capacity of the cell.

Detailed information about the aging cells and their testing procedures are listed in Tables 4 and 5, respectively. The *SOH* of the batteries ranged from 100% to 63.9% (Table 4), which covers the whole life cycle of commercially available lithium-ion batteries. The characterization procedures given in Table 5 mainly consist of EIS tests at a certain open-circuit voltage (OCV).

Table 4. Capacity and *SOH* of aging D-type cells.

Cell Number	D1	D2	D3	D4	D5	D6	D7
Capacity (Ah)	24.2	22.6	22.0	21.1	20.1	19.3	15.5
SOH (%)	100	93.4	90.6	87.2	82.8	79.5	63.9

Table 5. Characterization procedures of the aging D-type cells.

Step No.	Step Name	Duration	Current
1	Rest	180 min	
2	Discharge		I = 1/3 C
3	Rest	180 min	
4	Charge to 3.68 V		I = 1/20 C
5	Rest	180 min	
6	EIS test		
7	End		

4. Results and Discussion

In this section, the test results are given, the estimation results using the joint estimation method are provided, and a comparison of the C_{DC} and the C_{IC} is conducted. C_{DC} values of the cells with different capacities were estimated, and their relationship with the *SOH* of the cells was evaluated.

4.1. The Estimation Results of the DRT and the C_{DC}

Figure 4 shows the EIS results of Cells A, B, C and D. The EIS results are shifted in the y-direction for better visualization.

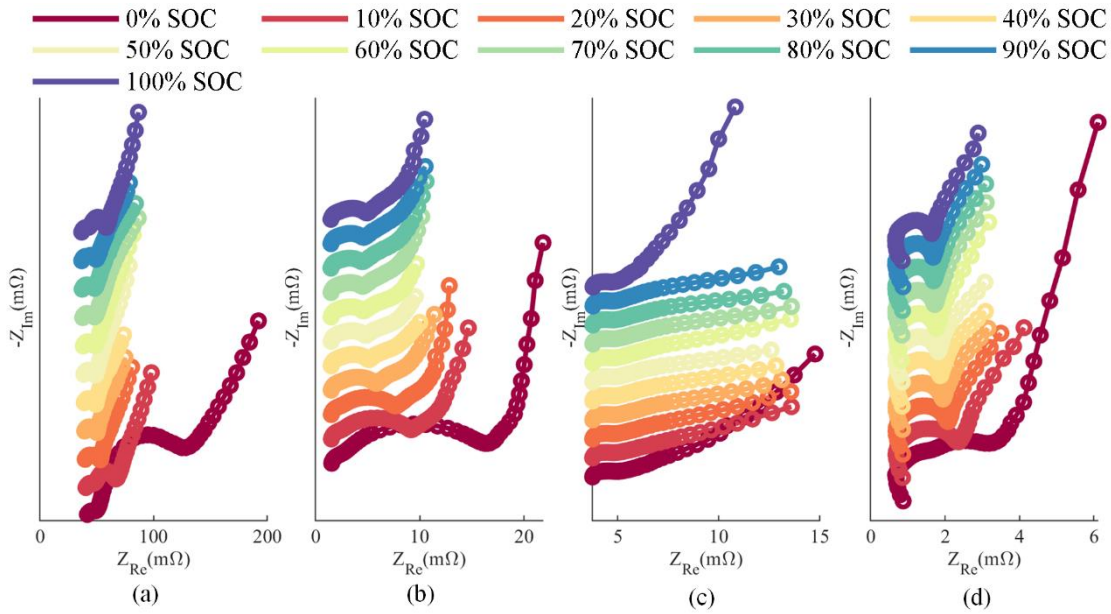

Figure 4. EIS results of (**a**) Cell A; (**b**) Cell B; (**c**) Cell C; and (**d**) Cell D at every 10% SOC.

The C_{DC} and the DRT were simultaneously estimated by the joint estimation method based on the shown EIS results. A comparison of the traditional DRT method and the proposed joint estimation method is shown in Figure 5, where the blue line shows the results obtained by the traditional DRT method, and the red one shows the results obtained by the proposed joint estimation method. The solid and dotted lines are the EIS results in different frequency bands. The frequency range of the solid lines was 2 kHz–2 mHz while the frequency range of the dotted lines was 2 kHz–20 mHz, which means that the solid line contains the low frequency (LF) and the dotted line does not. The C_{DC} cannot be accurately determined by the traditional DRT method, which can be seen from the highest peak in Figure 5. This peak is caused by the C_{DC}, and its height and position are affected by the frequency range of the EIS. The results of the proposed joint estimation method are hardly affected by the frequency range of the EIS. Therefore, the proposed joint estimation method can effectively solve the problem of determining the C_{DC} compared with the traditional DRT method.

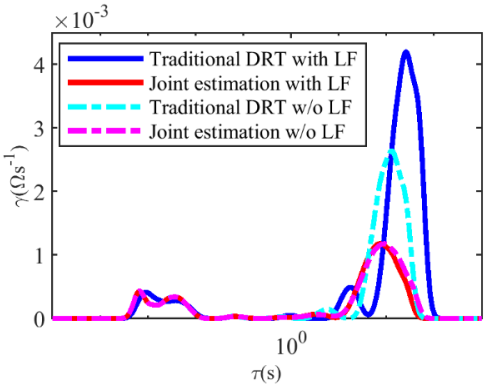

Figure 5. Joint estimation method compared with the traditional DRT method.

Figure 6 shows the results of the C_{DC} estimated by the joint estimation method (red crosses) and the ICA curves (blue lines). Here, the C_{DC} values estimated by the joint estimation method are compared with C_{IC} values obtained by ICA at the corresponding voltage according to Equation (2), as the traditional DRT method cannot provide the C_{DC}. The estimation C_{DC} values are close to the C_{IC} values at the corresponding voltage, indicating that the joint estimation method exhibits adequate

accuracy. The relative errors of the C_{DC} and C_{IC} values are shown in Figure 7. The relative errors are below 10% except for the individual points, indicating the method's sufficient accuracy.

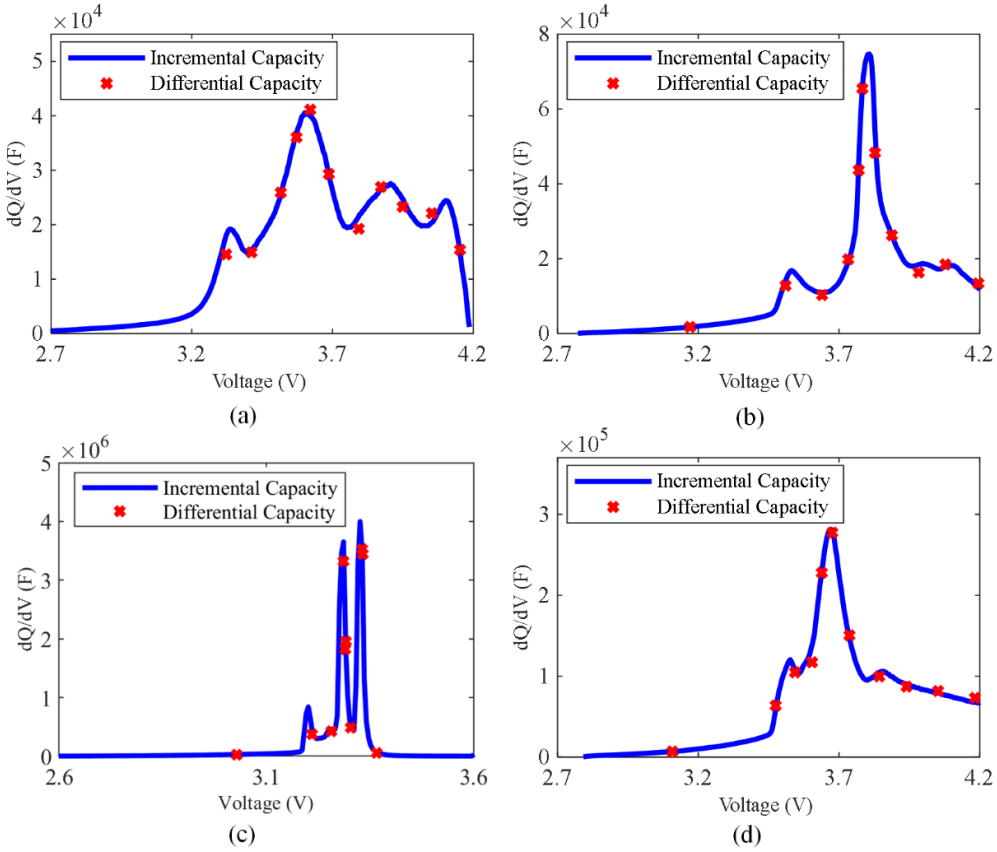

Figure 6. Identification results of the differential capacity C_{DC} compared with ICA for (**a**) Cell A; (**b**) Cell B; (**c**) Cell C; and (**d**) Cell D.

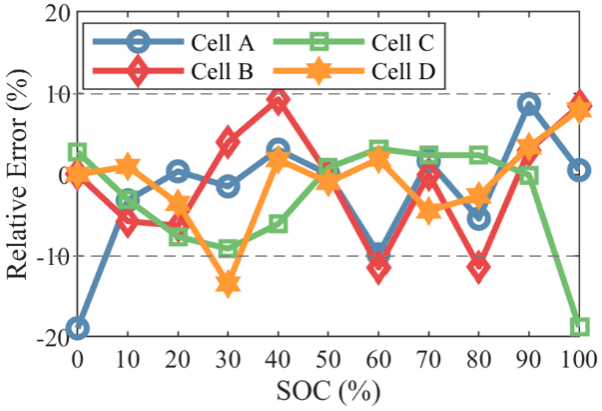

Figure 7. Relative errors between C_{DC}s and C_{IC}s.

4.2. SOH Evaluation Based on the Relationship between the C_{DC} and the Cell Capacity

The C_{DC} values of the aging D-type cells were estimated (Table 6). The red crosses shown in Figure 8 are the estimated C_{DC} values at different cell capacities. The relationship between C_{DC} and the cell capacity can be described by Equation (9):

$$Q = a_1 \exp(b_1 \cdot C_{DC}) + a_2 \exp(b_2 \cdot C_{DC}) \quad (9)$$

where Q is the capacity of the cell; a_1, a_2, b_1, and b_2 are fitting coefficients. In this paper, cftool provided by MATLAB is utilized for the fast parameter identification of Equation (9) as it can realize many types of linear and nonlinear curve fitting. The nonlinear least square (NLR) method is set, and the Levenberg-Marquardt algorithm is adopted to identify the fitting coefficients. The values of the fitting coefficients are listed in Table 7 for the D-type cells. The blue line shown in Figure 8 is the fitting curve of the C_{DC} values described by Equation (9), which provides an accurate fit. Subsequently, the *SOH* can be evaluated by combining Equations (8) and (9):

$$SOH = \frac{Q_{act}}{Q_{nom}} = \frac{a_1}{Q_{nom}} \exp(b_1 \cdot C_{DC}) + \frac{a_2}{Q_{nom}} \exp(b_2 \cdot C_{DC}) \quad (10)$$

Table 6. Differential capacity C_{DC} of the aging D-type cells.

Cell Number	D1	D2	D3	D4	D5	D6	D7
C_{DC} (10^5 F)	1.80	1.33	1.12	0.928	0.857	0.785	0.673

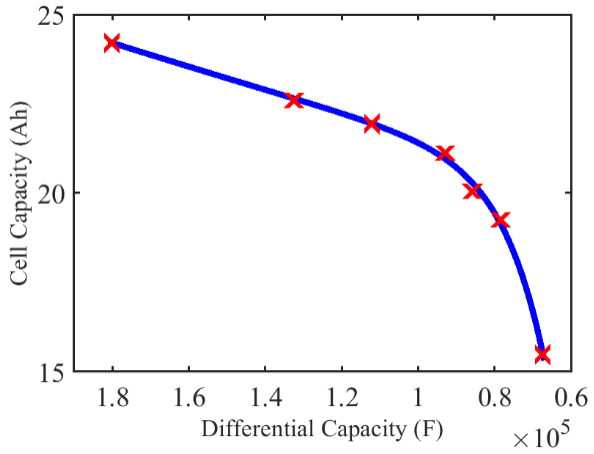

Figure 8. Relationship between C_{DC} and cell capacity.

Table 7. Fitting coefficients of the aging D-type cells.

Fitting Coefficient	a_1	a_2	b_1	b_2
Value	18.86	−2550	1.386×10^{-6}	-9.197×10^{-5}

The estimated *SOH* of the aging D-type cells given by Equation (10) and the relative errors between the real *SOH* and the estimated *SOH* are given in Table 8. These results show that the demonstrated *SOH* evaluation method exhibits adequate accuracy along the whole life cycle of the cells.

Table 8. SOH evaluation results of the aging D-type cells.

Cell Number	D1	D2	D3	D4	D5	D6	D7
Real SOH (%)	100	93.4	90.6	87.2	82.8	79.5	63.9
Estimated SOH (%)	100	93.6	90.7	86.5	83.8	79.1	64.0
Relative error (%)	0	0.23	0.02	0.80	−1.13	−0.51	0.05

Hence, the *SOH* of batteries of the same type can be evaluated only by EIS at a specific potential when a_1, a_2, b_1 and b_2 are obtained. It is worth noting that this study chose 3.68 V as the measured equilibrium potential for EIS, simply because the highest peak of the ICA is located at approximately 3.68 V. One can select this equilibrium potential arbitrarily as long as its corresponding ICA value

changes with the aging of the battery. If the measured equilibrium potential for EIS changes, the fitting coefficients of Equation (9) will change, but the structure of Equation (9) will not.

The EIS based SOH evaluation method is more efficient compared with the ICA based SOH evaluation method, which only needs impedance spectra rather than charging/discharging data of the battery.

5. Conclusions

The present work proposed a joint estimation method to estimate the differential capacity C_{DC} and the DRT simultaneously based on the EIS of lithium-ion batteries. Four types of commercially available lithium-ion batteries were tested to evaluate the joint estimation method and to verify the equivalence. Experimental data showed that the proposed joint estimation method outperforms the traditional method in the estimation of the C_{DC}. Moreover, the estimated C_{DC} values are consistent with the C_{IC} values obtained by ICA. Key points of this study are summarized as follows:

(1) A joint estimation method with Tikhonov regularization is proposed to simultaneously estimate the differential capacity C_{DC} and the DRT with the aim of minimizing the estimation errors and to obtain more information about the diffusion processes by EIS.
(2) The equivalence of the differential capacity C_{DC} and the incremental capacity C_{IC} was shown.
(3) An efficient state-of-health (SOH) evaluation method is demonstrated based on the relationship between the C_{DC} and the cell capacity.

The proposed joint estimation method can provide an intuitive understanding of the capacitive characteristics of lithium-ion batteries and can be used for SOH evaluation. Further research is being conducted to estimate the differential capacity C_{DC} from time-domain data for online applications.

Author Contributions: Conceptualization, G.Y. and X.F.; Data curation, M.Y. and X.H.; Investigation, D.G.; Methodology, D.G. and X.H.; Project administration, G.Y. and X.F.; Resources, G.Z.; Supervision, M.O.; Validation, L.L.; Writing-original draft, D.G.; Writing-review & editing, X.F. All authors have read and agreed to the published version of the manuscript.

Funding: This work was supported by the Ministry of Science and Technology of China [Grant No. 2016YFE0102200]; the National Key R&D Program of China [Grant No. 2016YFB0900302]; the National Natural Science Foundation of China [Grant No. 51706117 and U1564205]; the Science Program of State Grid Corporation of China [Grant No. 521702180003].

Conflicts of Interest: The authors declare no conflict of interest.

Nomenclature

$\boldsymbol{A'}$	approximation matrix of the DRT for the real part of the EIS
$\boldsymbol{A''}$	approximation matrix of the DRT for the imaginary part of the EIS
a, b	fitting coefficient of C_{DC} and Q
C_{DC}	differential capacity
C_{IC}	incremental capacity
g	distribution of the polarization resistance
j	imaginary unit
J	modified Tikhonov regularization function
I	current response
$\boldsymbol{M}$	regularization matrix
Q	capacity of the cell
Q_{act}	actual capacity of the present condition
Q_{nom}	nominal capacity of the cell
R_{ohm}	ohmic resistance

R_{pol}	polarization resistance
U	voltage excitation
$\boldsymbol{x}$	vector of the parameter for DRT approximation
Z_{DRT}	impedance model of the DRT
$Z^{\text{C}}_{\text{DRT}}$	DRT model considering differential capacity
Z_{exp}	experimental data of the EIS
$\boldsymbol{Z}^{\text{Re}}_{\text{exp}}$	real part of the experimental data
$\boldsymbol{Z}^{\text{Im}}_{\text{exp}}$	imaginary part of the experimental data
$\mathbf{1}$	column vector with n entries all equal to 1
λ	regularization coefficient
τ	characteristic time constants
ω	angular frequency
$\boldsymbol{\Omega}', \boldsymbol{\Omega}''$	frequency matrix of the DRT

Abbreviations

DDC	distribution function of the differential capacity
DDT	distribution of the diffusion times
DIA	differential impedance analysis
DRT	distribution of the relaxation times
ECM	equivalent-circuit model
EIS	electrochemical impedance spectroscopy
FS	full-scale
ICA	incremental capacity analysis
LFP	$LiFePO_4$
LMO	$LiMn_2O_4$
NCM	$LiNi_xCo_yMn_zO_2$
OCV	open-circuit voltage
PDF	probability density function
PHM	prognostics and health management
RC	resistor-capacitor
SOC	state of charge
SOFC	solid oxide fuel cell
SOH	state-of-health

Appendix A

The theoretical solution of the C_{DC} is:

$$C_{\text{DC}} = \lim_{\omega \to 0} \frac{1}{j\omega\left(\frac{U(\omega)}{I(\omega)} - R_{\text{ohm}} - R_{\text{pol}}(\omega)\right)} \tag{A1}$$

Equation (A1) can be written as Equation (A2) applying certain mathematical transformations:

$$C_{\text{DC}} = \lim_{\omega \to 0} \frac{1}{j\omega\frac{U(\omega)}{I(\omega)} - j\omega R_{\text{ohm}} - j\omega R_{\text{pol}}(\omega)} \tag{A2}$$

Then, the limit of the first term in Equation (A2) can be found as:

$$\lim_{\omega \to 0} j\omega\frac{U(\omega)}{I(\omega)} = \lim_{\omega \to 0} \frac{U(\omega)}{\frac{1}{j\omega}I(\omega)} \tag{A3}$$

Equation (A3) can be simplified to Equation (A4) by substituting $s = \frac{1}{j\omega}$, which is the Laplace Transformation of the Unit Step Function $1(t)$:

$$\lim_{\omega \to 0} j\omega\frac{U(\omega)}{I(\omega)} = \lim_{\omega \to 0} \frac{U(\omega)}{Q(\omega)} = \frac{\mathrm{d}U}{\mathrm{d}Q} \tag{A4}$$

The limits of the second and third terms in Equation (A2) are zero:

$$\lim_{\omega \to 0} j\omega R_{\text{ohm}} = 0 \tag{A5}$$

$$\lim_{\omega \to 0} j\omega R_{\text{pol}}(\omega) = 0 \tag{A6}$$

In conclusion, Equation (A2) can be approximated as:

$$C_{\text{DC}} \approx \frac{1}{\frac{\mathrm{d}U}{\mathrm{d}Q} - 0} = \frac{\mathrm{d}Q}{\mathrm{d}U} = C_{\text{IC}} \tag{A7}$$

which is equivalent to the incremental capacity C_{IC}.

References

1. Andre, D.; Meiler, M.; Steiner, K.; Wimmer, C.; Soczka-Guth, T.; Sauer, D. Characterization of high-power lithium-ion batteries by electrochemical impedance spectroscopy. I. Experimental investigation. *J. Power Sources* **2011**, *196*, 5334–5341. [CrossRef]
2. Andre, D.; Meiler, M.; Steiner, K.; Walz, H.; Soczka-Guth, T.; Sauer, D. Characterization of high-power lithium-ion batteries by electrochemical impedance spectroscopy. II: Modelling. *J. Power Sources* **2011**, *196*, 5349–5356. [CrossRef]
3. Nara, H.; Mukoyama, D.; Shimizu, R.; Momma, T.; Osaka, T. Systematic analysis of interfacial resistance between the cathode layer and the current collector in lithium-ion batteries by electrochemical impedance spectroscopy. *J. Power Sources* **2019**, *409*, 139–147. [CrossRef]
4. Gruet, D.; Delobel, B.; Sicsic, D.; Lucas, I.T.; Vivier, V. On the electrochemical impedance response of composite insertion electrodes–Toward a better understanding of porous electrodes. *Electrochim. Acta* **2019**, *295*, 787–800. [CrossRef]
5. Li, W.; Huang, Q.-A.; Yang, C.; Chen, J.; Tang, Z.; Zhang, F.; Li, A.; Zhang, L.; Zhang, J. A fast measurement of Warburg-like impedance spectra with Morlet wavelet transform for electrochemical energy devices. *Electrochim. Acta* **2019**, *322*, 134760. [CrossRef]
6. Rodríguez, A.; Plett, G.L.; Trimboli, M.S. Comparing four model-order reduction techniques, applied to lithium-ion battery-cell internal electrochemical transfer functions. *eTransportation* **2019**, *1*, 100009. [CrossRef]
7. Schichlein, H.; Müller, A.C.; Voigts, M.; Krügel, A.; Ivers-Tiffée, E. Deconvolution of electrochemical impedance spectra for the identification of electrode reaction mechanisms in solid oxide fuel cells. *J. Appl. Electrochem.* **2002**, *32*, 875–882. [CrossRef]
8. Klotz, D.; Schmidt, J.P.; Kromp, A.; Weber, A.; Ivers-Tiffée, E. The distribution of relaxation times as beneficial tool for equivalent circuit modeling of fuel cells and batteries. *ECS Trans.* **2012**, *41*, 25–33.
9. Oz, A.; Hershkovitz, S.; Belman, N.; Tal-Gutelmacher, E.; Tsur, Y. Analysis of impedance spectroscopy of aqueous supercapacitors by evolutionary programming: Finding DFRT from complex capacitance. *Solid State Ionics* **2016**, *288*, 311–314. [CrossRef]
10. Helseth, L. Modelling supercapacitors using a dynamic equivalent circuit with a distribution of relaxation times. *J. Energy Storage* **2019**, *25*, 100912. [CrossRef]
11. Illig, J.; Ender, M.; Chrobak, T.; Schmidt, J.P.; Klotz, D.; Ivers-Tiffée, E. Separation of charge transfer and contact resistance in LiFePO4-cathodes by impedance modeling. *J. Electrochem. Soc.* **2012**, *159*, A952–A960. [CrossRef]
12. Illig, J.; Schmidt, J.P.; Weiss, M.; Weber, A.; Ivers-Tiffée, E. Understanding the impedance spectrum of 18650 LiFePO4-cells. *J. Power Sources* **2013**, *239*, 670–679. [CrossRef]
13. Sabet, P.S.; Sauer, D.U. Separation of predominant processes in electrochemical impedance spectra of lithium-ion batteries with nickelmanganesecobalt cathodes. *J. Power Sources* **2019**, *425*, 121–129. [CrossRef]
14. Rahbari, O.; Omar, N.; Van Mierlo, J.; A Rosen, M.; Coosemans, T.; Berecibar, M. Electric Vehicle Battery Lifetime Extension through an Intelligent Double-Layer Control Scheme. *Energies* **2019**, *12*, 1525. [CrossRef]
15. Waag, W.; Käbitz, S.; Sauer, D.U. Experimental investigation of the lithium-ion battery impedance characteristic at various conditions and aging states and its influence on the application. *Appl. Energy* **2013**, *102*, 885–897. [CrossRef]

16. Spinner, N.S.; Love, C.T.; Rose-Pehrsson, S.L.; Tuttle, S.G. Expanding the operational limits of the single-point impedance diagnostic for internal temperature monitoring of lithium-ion batteries. *Electrochim. Acta* **2015**, *174*, 488–493. [CrossRef]
17. Gordon, I.A.J.; Grugeon, S.; Takenouti, H.; Tribollet, B.; Armand, M.; Davoisne, C.; Débart, A.; Laruelle, S. Electrochemical Impedance Spectroscopy response study of a commercial graphite-based negative electrode for Li-ion batteries as function of the cell state of charge and ageing. *Electrochim. Acta* **2017**, *223*, 63–73. [CrossRef]
18. Van Nguyen, D.; Limmer, S.; Yang, K.; Olhofer, M.; Bäck, T. Modeling and Prediction of Remaining Useful Lifetime for Maintenance Scheduling Optimization of a Car Fleet. *Int. J. Perform. Eng.* **2019**, *15*, 2318–2328.
19. Limmer, S. Evaluation of Optimization-Based EV Charging Scheduling with Load Limit in a Realistic Scenario. *Energies* **2019**, *12*, 4730. [CrossRef]
20. Schoenleber, M.; Ivers-Tiffée, E. Approximability of impedance spectra by RC elements and implications for impedance analysis. *Electrochem. Commun.* **2015**, *58*, 15–19. [CrossRef]
21. Gantenbein, S.; Weiss, M.; Ivers-Tiffée, E. Impedance based time-domain modeling of lithium-ion batteries: Part I. *J. Power Sources* **2018**, *379*, 317–327. [CrossRef]
22. Wang, X.; Wei, X.; Dai, H. Estimation of state of health of lithium-ion batteries based on charge transfer resistance considering different temperature and state of charge. *J. Energy Storage* **2019**, *21*, 618–631. [CrossRef]
23. Collin, R.; Miao, Y.; Yokochi, A.; Enjeti, P.; von Jouanne, A. Advanced Electric Vehicle Fast-Charging Technologies. *Energies* **2019**, *12*, 1839. [CrossRef]
24. Pastor-Fernández, C.; Uddin, K.; Chouchelamane, G.H.; Widanage, W.D.; Marco, J. A Comparison between Electrochemical Impedance Spectroscopy and Incremental Capacity-Differential Voltage as Li-ion Diagnostic Techniques to Identify and Quantify the Effects of Degradation Modes within Battery Management Systems. *J. Power Sources* **2017**, *360*, 301–318. [CrossRef]
25. Sun, B.; Bian, J.; Ruan, H.; Zhang, W.; Ren, P.; Cong, X. Modeling Study for Li-ion Batteries Considering High-frequency Inductance Characteristics Based on Electrochemical Impedance Spectroscopy. *DEStech Trans. Environ. Energy Earth Sci.* **2018**. [CrossRef]
26. Cheng, C.-S.; Chung, H.S.-H.; Lau, R.W.-H.; Hong, K.Y.-W. Experimental Assessment and Stability Analysis of a Discrete-Time Battery Model with Multiple Constant Phase Elements. In Proceedings of the 2019 IEEE Applied Power Electronics Conference and Exposition (APEC), Anaheim, CA, USA, 17–21 March 2019; pp. 1090–1097.
27. Tomaszewska, A.; Chu, Z.; Feng, X.; O'Kane, S.; Liu, X.; Chen, J.; Ji, C.; Endler, E.; Li, R.; Liu, L. Lithium-ion battery fast charging: A review. *eTransportation* **2019**, *1*, 100011. [CrossRef]
28. Schmidt, J.P.; Chrobak, T.; Ender, M.; Illig, J.; Klotz, D.; Ivers-Tiffée, E. Studies on LiFePO4 as cathode material using impedance spectroscopy. *J. Power Sources* **2011**, *196*, 5342–5348. [CrossRef]
29. Wan, T.H.; Saccoccio, M.; Chen, C.; Ciucci, F. Influence of the discretization methods on the distribution of relaxation times deconvolution: Implementing radial basis functions with DRTtools. *Electrochim. Acta* **2015**, *184*, 483–499. [CrossRef]
30. Sabet, P.S.; Stahl, G.; Sauer, D.U. Non-invasive investigation of predominant processes in the impedance spectra of high energy lithium-ion batteries with Nickel-Cobalt-Aluminum cathodes. *J. Power Sources* **2018**, *406*, 185–193. [CrossRef]
31. Zhou, X.; Pan, Z.; Han, X.; Lu, L.; Ouyang, M. An easy-to-implement multi-point impedance technique for monitoring aging of lithium ion batteries. *J. Power Sources* **2018**, *417*, 188–192. [CrossRef]
32. Zhou, X.; Huang, J.; Pan, Z.; Ouyang, M. Impedance characterization of lithium-ion batteries aging under high-temperature cycling: Importance of electrolyte-phase diffusion. *J. Power Sources* **2019**, *426*, 216–222. [CrossRef]
33. Boukamp, B.A. Derivation of a Distribution Function of Relaxation Times for the (fractal) Finite Length Warburg. *Electrochim. Acta* **2017**, *252*, 154–163. [CrossRef]
34. Malkow, K.T. A theory of distribution functions of relaxation times for the deconvolution of immittance data. *J. Electroanal. Chem.* **2019**, *838*, 221–231. [CrossRef]
35. Schmidt, J.P.; Berg, P.; Schönleber, M.; Weber, A.; Ivers-Tiffée, E. The distribution of relaxation times as basis for generalized time-domain models for Li-ion batteries. *J. Power Sources* **2013**, *221*, 70–77. [CrossRef]
36. Schichlein, H.; Feuerstein, M.; Müller, A.; Weber, A.; Krügel, A.; Ivers-Tiffée, E. System identification: A new modelling approach for SOFC single cells. *ECS Proc. Vol.* **1999**, *1999*, 1069–1077. [CrossRef]

37. Oldenburger, M.; Bedürftig, B.; Gruhle, A.; Grimsmann, F.; Richter, E.; Findeisen, R.; Hintennach, A. Investigation of the low frequency Warburg impedance of Li-ion cells by frequency domain measurements. *J. Energy Storage* **2019**, *21*, 272–280. [CrossRef]
38. Ciucci, F. Modeling Electrochemical Impedance Spectroscopy. *Curr. Opin. Electrochem.* **2018**, *13*, 132–139. [CrossRef]
39. Schönleber, M.; Ivers-Tiffée, E. The Distribution Function of Differential Capacity as a new tool for analyzing the capacitive properties of Lithium-Ion batteries. *Electrochem. Commun.* **2015**, *61*, 45–48. [CrossRef]
40. Song, J.; Bazant, M.Z. Electrochemical impedance imaging via the distribution of diffusion times. *Phys. Rev. Lett.* **2018**, *120*, 116001. [CrossRef]
41. Vladikova, D.; Stoynov, Z. Secondary differential impedance analysis–a tool for recognition of CPE behavior. *J. Electroanal. Chem.* **2004**, *572*, 377–387. [CrossRef]
42. Vladikova, D.; Kilner, J.; Skinner, S.; Raikova, G.; Stoynov, Z. Differential impedance analysis of single crystal and polycrystalline yttria stabilized zirconia. *Electrochim. Acta* **2006**, *51*, 1611–1621. [CrossRef]
43. Dubarry, M.; Svoboda, V.; Hwu, R.; Liaw, B.Y. Incremental capacity analysis and close-to-equilibrium OCV measurements to quantify capacity fade in commercial rechargeable lithium batteries. *Electrochem. solid. State. Lett.* **2006**, *9*, A454–A457. [CrossRef]
44. Feng, X.; Li, J.; Ouyang, M.; Lu, L.; Li, J.; He, X. Using probability density function to evaluate the state of health of lithium-ion batteries. *J. Power Sources* **2013**, *232*, 209–218. [CrossRef]
45. Saccoccio, M.; Wan, T.H.; Chen, C.; Ciucci, F. Optimal regularization in distribution of relaxation times applied to electrochemical impedance spectroscopy: Ridge and Lasso regression methods-A theoretical and experimental Study. *Electrochim. Acta* **2014**, *147*, 470–482. [CrossRef]
46. Ciucci, F.; Chen, C. Analysis of electrochemical impedance spectroscopy data using the distribution of relaxation times: A Bayesian and hierarchical Bayesian approach. *Electrochim. Acta* **2015**, *167*, 439–454. [CrossRef]
47. Han, X.; Lu, L.; Zheng, Y.; Feng, X.; Li, Z.; Li, J.; Ouyang, M. A review on the key issues of the lithium ion battery degradation among the whole life cycle. *eTransportation* **2019**, *1*, 100005. [CrossRef]
48. Tian, J.; Xiong, R.; Shen, W. A review on state of health estimation for lithium ion batteries in photovoltaic systems. *eTransportation* **2019**, *2*, 100028. [CrossRef]
49. Zhang, Y.; Xiong, R.; He, H.; Qu, X.; Pecht, M. Aging characteristics-based health diagnosis and remaining useful life prognostics for lithium-ion batteries. *eTransportation* **2019**, *1*, 100004. [CrossRef]
50. Ren, D.; Hsu, H.; Li, R.; Feng, X.; Guo, D.; Han, X.; Lu, L.; He, X.; Gao, S.; Hou, J.; et al. A comparative investigation of aging effects on thermal runaway behavior of lithium-ion batteries. *eTransportation* **2019**, *2*, 100034. [CrossRef]
51. Ali, M.U.; Zafar, A.; Nengroo, S.H.; Hussain, S.; Park, G.-S.; Kim, H.-J. Online Remaining Useful Life Prediction for Lithium-Ion Batteries Using Partial Discharge Data Features. *Energies* **2019**, *12*, 4366. [CrossRef]